# Isolation of the regions of potential significance in fine-structure transitions using adiabatic and functional sensitivity analyses: A comparative investigation with application to $Na(^2P_{1/2})+He \rightarrow Na(^2P_{3/2})+He$ and $Na(^2P_{1/2})+Ar \rightarrow Na(^2P_{3/2})+Ar$

D. A. Padmavathi and Manoj K. Mishra
*Department of Chemistry, Indian Institute of Technology, Powai, Bombay 400 076, India*

Herschel Rabitz
*Department of Chemistry, Princeton University, Princeton, New Jersey 08544*

(Received 31 March 1994)

The first-order functional sensitivity densities $\delta \ln\sigma_{1/2\rightarrow 3/2}(E)/\delta \ln W_{|\Lambda|}(R)$ are employed to assess the role of structure in the potential-energy curves $W_0(^2\Sigma)$ and $W_1(^2\Pi)$ mediating the fine-structure transition $Na(^2P_{1/2})+He \rightarrow Na(^2P_{3/2})+He$ and $Na(^2P_{1/2})+Ar \rightarrow Na(^2P_{3/2})+Ar$. The sensitivity density profiles $\delta \ln\sigma_{1/2\rightarrow 3/2}(E)/\delta \ln W_{|\Lambda|}(R)$ for the two systems reveal that regions of significance differ widely for the $^2\Sigma$ and $^2\Pi$ curves. The results suggest that prevalent mechanistic explanations from adiabatic analyses have limitations in terms of the ultimate significance of the identified kinematic coupling over well demarcated radial and angular coupling regions. The functional sensitivity analysis is shown to permit a full deconvolution of the collision cross section's dependence on the features in the individual $^2\Sigma$ and $^2\Pi$ curves as opposed to the adiabatic analysis where only the features in $[W_0(R)\text{-}W_1(R)]$ are deemed critical to the collisional outcome.

PACS number(s): 34.20.−b

## I. INTRODUCTION

Collisional fine-structure transitions are known to be extremely sensitive to the features in the underlying potential-energy curves [1–18]. A conceptually simple and direct means for gaining such insight is done by recalculating the collision cross sections using many different curves for the same system [1–6]. However, such an approach is not only computationally demanding but can never be exhaustive in its scope. A more physically motivated and economic technique is the adiabatic analysis where the total Hamiltonian is expressed in the basis that locally diagonalizes the sum of electrostatic, rotational, and spin-orbital components, and the nonadiabatic source of coupling comes from the familiar radial derivative terms [4–15]. Large coupling in this basis denotes the internuclear region where the adiabatic eigenfunctions are changing rapidly and one type of competing mechanism for nonadiabatic coupling is given way to the dominance of a different coupling scheme. This method of isolation of the regions of potential significance has provided valuable insights into the regions of potential curves responsible for fine-structure transitions and the different mechanisms that trigger these transitions [4-18] by examining the kinematic coupling structure of the total Hamiltonian in a fully adiabatic basis.

Another technique that directly probes the role of potential-energy curves in nonadiabatic collisions is functional sensitivity analysis [19], when the full dynamical dependence of collision cross sections $\sigma([V])$ on the functional form of the underlying potential-energy surface(s) $V(R)$ is directly quantified in detail through a functional expansion,

$$\delta\sigma=\sigma([V+\delta V])-\sigma([V])\approx\int dR\frac{\delta\sigma}{\delta V(R)}\delta V(R)\ , \quad (1)$$

where $R$ denotes generic coordinate space variables and the first-order functional sensitivity density $\delta\sigma/\delta V(R)$ serves as the role of a weight function in Eq. (1). A large magnitude of $\delta\sigma/\delta V(R)$ implies a region of importance and the cross section is sensitive to changes in potential(s) in this region. On the other hand, regions with small $\delta\sigma/\delta V(R)$ denote areas with little significance in the determination of the cross section. The direct calculation of functional sensitivity densities $\delta\sigma/\delta V(R)$ in the close-coupling approach requires only a minor extension and expense beyond the cross-section calculations alone and has been advantageously applied to determine regions of potential curves critical to diverse dynamical processes [15,19–23].

In an earlier paper [15] both functional sensitivity analysis and adiabatic analysis were utilized to probe the regions of potential significance in the fine-structure transition $H^+ + F(^2P_{1/2}) \rightarrow H^+ + F(^2P_{3/2})$. The dependence of the collisional cross section $\sigma_{1/2\rightarrow 3/2}$ on the $^2\Sigma$ and $^2\Pi$ curves was found to be similar and the significant regions of the two curves are almost identical [15] as determined by both the adiabatic and functional sensitivity analyses. Contrary to the correlated response by the two curves seen in this case, our experience with other systems [20,21] shows that the regions of potential significance may vary widely for the different potential-energy curves and we have suggested that the identity in the response to variations in both the curves may only be because of the domination of electrostatic interactions by the unusually strong spin-orbit coupling (spin-orbit coupling constant $a_F=422\ cm^{-1}$) in the fluorine atom. In systems with small spin-orbit coupling, e.g., the fine-structure transi-

 

tion induced in Na by collision with a rare gas [14,24,25] (spin-orbit coupling constant $a_{Na}=17.2$ cm$^{-1}$) the response to variations in the individual curves may be completely different for the underlying $^2\Sigma$ and $^3\Pi$ curves. Furthermore, as discussed earlier [15] the underlying physics dictated by Schrödinger's equation poses a boundary-value problem, and coupling in one location may strongly influence coupling elsewhere and an examination of only the local kinematic structure of the coupling matrix elements could be misleading. Only an investigation of the solution of Schrödinger's equation through sensitivity analysis can reveal the *hidden dynamic* couplings and provide the full and individual response of the collision cross section to the underlying potential curves. A deconvolution of the dependence of the cross section on features in the individual curves is not possible through adiabatic analysis. A deciphering of the role of individual curves is critical, for example, towards determining if the cross-section data may be inverted to recover or improve the underlying potential.

To clarify these issues it is useful to perform a functional sensitivity analysis of the role of potential features in fine-structure transitions for systems where exhaustive adiabatic analysis is available and the spin-orbit coupling constant is not unusually large to dominate electrostatic interactions. The alkali atom or alkaline earth atom plus rare-gas collisions inducing fine-structure transitions in the metal has been studied extensively [1,4,6–9,12–14,17,24–26]. In particular, the fine-structure transition in Na+He and Na+Ar has been analyzed in exhaustive detail by Lemoine, Robbe, and Pouilly [14]. In this paper we present results from a functional sensitivity analysis of the same two systems to examine the complementary strengths of these two techniques.

The methodology of functional sensitivity and adiabatic analyses of fine-structure transitions has been discussed in great detail elsewhere [4,14,15]. In Sec. II therefore, we present only a skeletal outline of the computational formulas needed for calculation of the close-coupling sensitivities and nonadiabatic coupling matrix elements. Analysis of the functional sensitivity profiles and correlation of the features therein with results from a fully adiabatic analysis is presented in Sec. III and finally some concluding remarks are given in Sec. IV.

## II. METHOD

The collision cross section $\sigma_{1/2\to3/2}(E)$ for the $^2P_{1/2}\to{}^2P_{3/2}$ fine-structure transition is given by [4,8,26]

$$\sigma_{1/2\to3/2}(E)=\frac{\pi}{2k_{1/2}^2}\sum_p\sum_J(2J+1)(|\mathbf{S}_{31}^J|^2+|\mathbf{S}_{32}^J|^2) \tag{2}$$

where $p$ denotes parity [27] and the scattering matrix $\mathbf{S}^J$ for each value of the total angular momentum $J$ for parity $(-1)^{J+1/2}$ (parity $f$) is indexed by the compound indices $1(j=\frac{3}{2};l=J+\frac{3}{2})$, $2(j=\frac{3}{2};l=J-\frac{1}{2})$, and $3(j=\frac{1}{2};l=J-\frac{1}{2})$ and for opposite parity $(-1)^{J-1/2}$ (parity $e$) the compound indices 1,2,3 denote the channel states $1(j=\frac{3}{2};l=J-\frac{3}{2})$, $2(j=\frac{3}{2};l=J+\frac{1}{2})$, and $3(j=\frac{1}{2};l=J+\frac{1}{2})$, respectively [4,14,15,27,28]. The total angular momentum operator $\vec{J}=\vec{j}+\vec{l}$, where $\vec{l}$ is the angular momentum of the relative nuclear motion and the total electronic angular-momentum operator $\vec{j}=\vec{L}+\vec{S}$, where $\vec{L}$ and $\vec{S}$ are the electronic orbital angular-momentum and spin angular-momentum operators, respectively.

The functional sensitivity density is given by

$$\frac{\delta\sigma_{1/2\to3/2}(E)}{\delta W_{|\Lambda|}(R)}=\frac{\pi}{k_{1/2}^2}\sum_p\sum_J\sum_{i=1}^3\sum_{j=1}^3(2J+1)\mathrm{Re}\left[(\mathbf{S}_{31}^J)^*\int\frac{\delta\mathbf{S}_{31}^J(E)}{\delta V_{ij}(R')}\frac{\delta V_{ij}(R')}{\delta W_{|\Lambda|}(R)}dR'+(\mathbf{S}_{32}^J)^*\times\int\frac{\delta\mathbf{S}_{32}^J(E)}{\delta V_{ij}(R')}\frac{\delta V_{ij}(R')}{\delta W_{|\Lambda|}(R)}dR'\right], \tag{3}$$

where the compound indices $i$ and $j$ for each parity $p$ denote the channel states defined previously and $|\Lambda|$ is the eigenvalue of $\vec{R}\cdot\vec{l}$ [15]. In terms of these compound indices $i$ and $j$, taking $R_m$ to be the $m$th point on the solution grid, one may show that

$$\frac{\delta\sigma_{1/2\to3/2}(E)}{\delta W_{|\Lambda|}(R_m)}=\frac{2\pi^2}{k_{1/2}^2}\sum_p\sum_J\sum_i\sum_j(2J+1)\mathrm{Im}[(\mathbf{S}_{31}^J)^*\mathbf{U}_m^{J+}(i,1)\mathbf{U}_m^{J+}(j,3)+(\mathbf{S}_{32}^J)^*\mathbf{U}_m^{J+}(i,2)\mathbf{U}_m^{J+}(j,3)]\times[\delta_{\Lambda,0}\mathbf{C}_{i,j}^J+\delta_{|\Lambda|,1}(\delta_{i,j}-\mathbf{C}_{i,j}^J)], \tag{4}$$

where $\mathbf{U}^+(i,j)$ is the $i$th component of the outgoing wave in channel $j$ and the $\mathbf{C}_{i,j}^J$ have been tabulated elsewhere [14,27]. Equation (3) serves as the working relation for the computation of functional sensitivity densities reported in this paper.

The total Hamiltonian matrix ($\mathbf{W}^J$) in the asymptotic diabatic basis used for the formulation of the coupled channel equations is given by [1,4,14]

$$\mathbf{W}^J(R)_{jl,j'l'}=\delta_{jl,j'l'}\left[\mathcal{E}_j+\frac{l(l+1)}{2\mu R^2}\right]+V_{jl,j'l'}^J(R), \tag{5}$$

and has been catalogued earlier [27,29]. After transformation to the adiabatic eigenbasis $\mathbf{A}$ of $\mathbf{W}$ defined by

$$\mathbf{A}^T\mathbf{W}\mathbf{A}=\lambda, \tag{6}$$

where $\lambda$ is the diagonal matrix of eigenvalues of $\mathbf{W}$, the

radial kinetic operator is no longer diagonal, and the adiabatic analysis typically consists of examining the radial dependence of the first derivative coupling matrix elements $G_{ij}$ defined by [4,13,14].

$$\mathbf{G}=\mathbf{A}^T\frac{d}{dR}\mathbf{A}\ . \tag{7}$$

Usually, large nonadiabatic coupling corresponds to regions of $R$ where the adiabatic wave functions, expressed in the diabatic basis, are changing rapidly and are taken to denote areas critical to the fine-structure transitions.

## III. RESULTS AND DISCUSSION

The molecular potential curves $^2\Sigma(W_0)$ and $^2\Pi(W_1)$ for Na($3\,^2P$)–He and Na($3\,^2P$)–Ar are the same as those employed by Lemoine, Robbe, and Pouilly [14] and are displayed in Figs. 1(a) and 1(b). Figures 1(c) and 1(d) display the difference $[^2\Sigma(R)-{}^2\Pi(R)]$ for the two systems. The crossing point $R_c$ and the internuclear distance $R_r$ for which $^2\Sigma(R_r)-{}^2\Pi(R_r)=\Delta\epsilon$ (the spin-orbit splitting in Na) are at 18.33 and 13.89 a.u. for Na-He [Fig. 1(c)] and 12.20 and 11.64 a.u. for Na-Ar [Fig. 1(d)]. The $^2\Sigma$ state has a shallow well and the $^2\Pi$ a broader deeper well for both the systems. The $^2\Pi$ and $^2\Sigma$ wells for Na-Ar are, however, broader than those for Na-He. The shallow $^2\Sigma$ wells in both Na-Ar and Na-He curves may be responsible for the sharp resonances [21,24] near the threshold in the energy profile of total intramultiplet cross sections displayed in Fig. 2. The steeper slope of $[^2\Sigma(R_r)-{}^2\Pi(R_r)]$ near $R_r$ for Na-Ar limits the range of $R$ values (or impact parameters) for which $^2\Sigma(R_r)-{}^2\Pi(R_r)\simeq\Delta\epsilon$ and thereby angular momenta and total collisional energies over which fine-structure transitions will be triggered. This feature should lead to a narrower radial coupling region and narrower maxima in

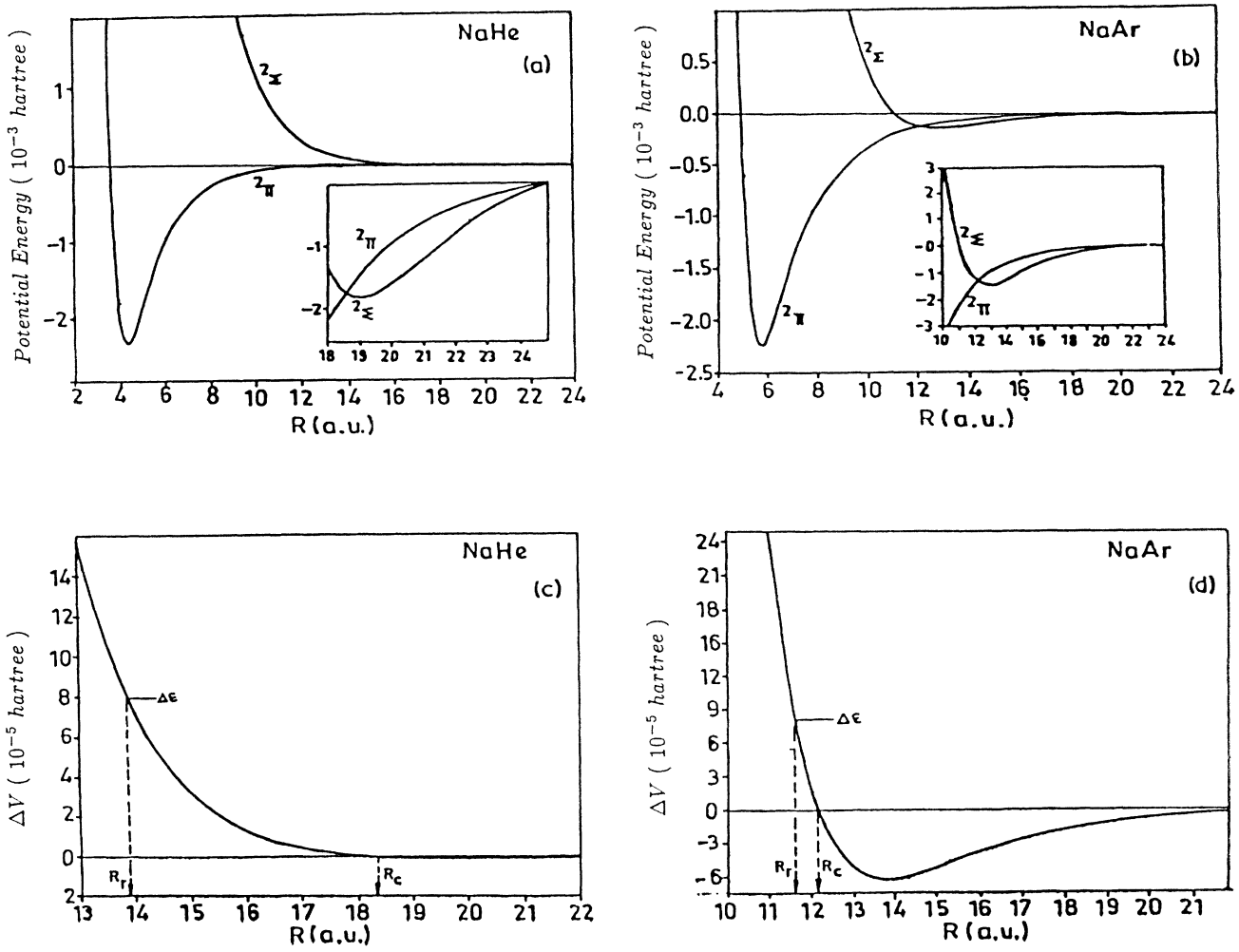


FIG. 1. The molecular potential curves [14] $^2\Sigma(W_0)$ and $^2\Pi(W_1)$ for (a) Na ($3\,^2P$)–He and (b) Na($3\,^2P$)–Ar. A magnified plot of the $^2\Sigma$ and $^2\Pi$ curves is displayed in the inset where the energy values on the vertical axis are in units of $10^{-6}$ a.u. for Na($3\,^2P$)–He and in units of $10^{-4}$ a.u. for Na ($3\,^2P$)–Ar. (c) and (d) display the difference of $^2\Sigma(R)-{}^2\Pi(R)$ as a function of internuclear distance $R$ for Na-He and Na-Ar, respectively. The crossing point $R_c$ and the distance $R_r$ at which $^2\Sigma(R_r)-{}^2\Pi(R_r)=\Delta\epsilon$ (the spin-orbit splitting) are at 18.33 and 13.89 a.u. for Na-He (c) and 12.20 and 11.64 a.u. for Na-Ar (d).

$\sigma_{1/2\to3/2}(E)$ vs $E$ plots for Na-Ar as opposed to Na-He, where the less steep slope near $R_r$ permits a broader span for the coupling region and a broad maxima in the total cross-section profile. These systematic differences are seen in all the figures to be discussed and the narrow (broad) maxima for Na-Ar (Na-He) is clearly seen in Fig. 2. Our calculated intramultiplet cross sections agree with the values reported by Lemoine, Robbe, and Pouilly [14].

The total intramultiplet cross section may also be partitioned as the sum of the parity $e$ and parity $f$ contributions $\sigma_{1/2\to3/2}(E)=\sigma^e_{1/2\to3/2}(E)+\sigma^f_{1/2\to3/2}(E)$, and the curves show that the contribution from $e$ levels dominates except in the immediate vicinity of the threshold region for the Na-Ar system. The nonadiabatic coupling matrix elements for the $^2P_{1/2}\to{}^2P_{3/2}$ fine-structure transitions have been tabulated in many places [4,14,27,29]. The angular contribution to nonadiabaticity is parity dependent and due to its larger reduced mass; the rotational contribution and consequently the parity dependence should be more acute for Na-Ar. This sharp difference in parity dependence over a large range of collisional energies is seen in the $\sigma^e_{1/2\to3/2}(E)$ and $\sigma^f_{1/2\to3/2}(E)$ contributions for Na-Ar.

The dependence on internuclear distance of the absolute values of nonadiabatic matrix elements $G_{13}$ and $G_{12}$ for the collision system Na+He for different values of $J$ is shown in Fig. 3. A magnified plot of the curve crossing ($R_c=18.33$ a.u.) region is displayed in the insets. The structure seen in the inset in the immediate vicinity of the curve crossing point was not resolved in the earlier analysis [14]. The maxima in almost all the coupling elements is in the pure radial coupling region centered on $R_r$, and the comparative parity independence of $G_{13}$ and sharp parity dependence of $G_{12}$ for large $J$ values has been explained adequately by Lemoine, Robbe, and Pouilly in terms of the presence of a centrifugal barrier for adiabatic states 1 and 3 in $e$ parity [14]. The position of maxima near $R_r$ highlights the important role of pure radial coupling in triggering fine-structure transitions and lack of importance of the curve crossing region for Na-He. The structure near the crossing point where the coupling elements rise rapidly makes us anticipate that for systems where $R_r$ is close to $R_c$ (e.g., for Na-Ar) coupling should be strong near $R_c$ and this is indeed seen in the plots of nonadiabatic elements for Na-Ar (Fig. 5). The large maxima for $J=100.5$ in Fig. 3(d) has been attributed to rotationally induced outer radial coupling, spanning the internuclear distances where the difference between the centrifugal barriers between the adiabatic levels 1 and 2 equals $\Delta\epsilon$, i.e., $\Delta\epsilon=\hbar^2(4J+\frac{3}{2})/2\mu R^2$ or for $R\simeq\hbar[(4J+\frac{3}{2})/2\mu\Delta\epsilon]^{1/2}$.

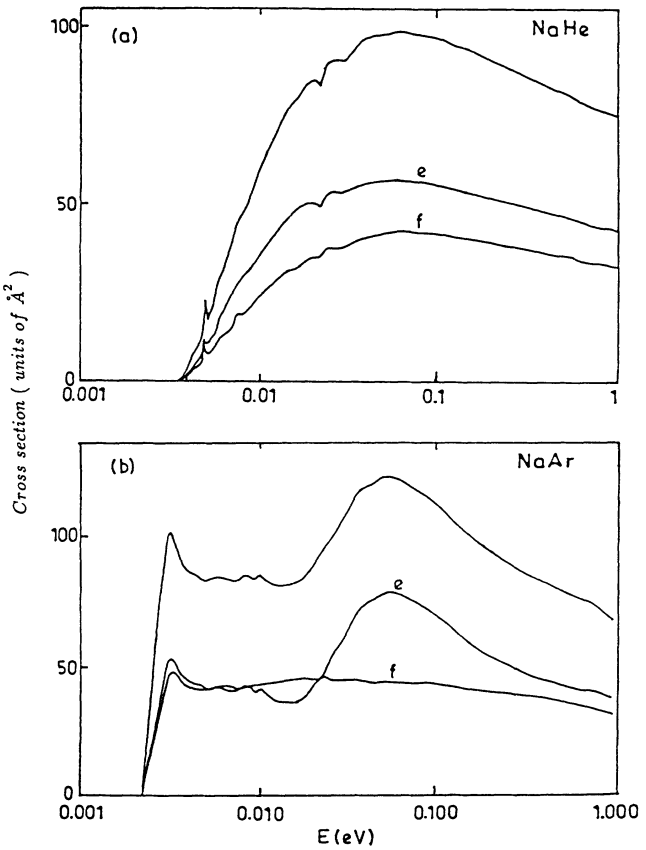


FIG. 2. The total intramultiplet inelastic cross sections $\sigma_{1/2\to3/2}(E)$ for (a) Na($3\,^2P$)–He and (b) Na($3\,^2P$)–Ar. The parity $e$ and parity $f$ cross sections are also displayed. The curves show that the contribution from $e$ levels dominates.

The total cross section $\sigma_{1/2\to3/2}(E)$ may also be analyzed in terms of partial cross sections $\sigma^J_{1/2\to3/2}(E)$ where $\sigma_{1/2\to3/2}(E)=\sum_J\sigma^J_{1/2\to3/2}(E)$. Due to the small reduced mass of Na-He the contribution of $J$ values higher than 60 is negligible [14] and the unusually large nonadiabatic coupling for $J=100.5$ in the outer radial coupling region $R\simeq20.5$ centered far from $R_r$ should be of little significance for the Na-He collision dynamics. This is made apparent by Fig. 4 where the log-normalized functional sensitivity density profiles $\delta\ln\sigma_{1/2\to3/2}(E)/\delta\ln W_0(R)$ and $\delta\ln\sigma_{1/2\to3/2}(E)/\delta\ln W_1(R)$ at collisional energies $E=0.06$ and 0.20 a.u. for Na+He have been plotted and the extreme significance of the region centered at $R\simeq20.5$ a.u. in Fig. 3(d) identified by the static adiabatic analysis is seen to be missing from the dynamic sensitivities plotted here. The region of potential significance is almost the same as that identified by the adiabatic analysis in Figs. 3(a)–3(c). However, in contrast to the comparative parity independence of the coupling matrix elements from the adiabatic analysis (even $G^e_{12}$ and $G^f_{12}$ are similar for small $J$) the contribution from parity $e$ dominates all sensitivity profiles mirroring its dominant contribution to total cross section seen in Fig. 2.

The sensitivities are zero in the nonclassical region for each curve, and the ringing structure in the area of the deep well in the $^2\Pi$ curve is in tune with our earlier analyses [20,21], and the frequency of this ringing increases with an increase in the total collisional energy $E$ as expected. Though the pure radial coupling region centered at $R_r$ is clearly significant, smaller internuclear distances far removed from $R_r$ are equally significant and dominate at higher energy for the $^2\Sigma$ curve [Fig. 4(c)] and at both the energies for the $^2\Pi$ curve [(b) and (d)]. On the whole, the $R<R_r$ region seems more significant and electrostat-

ic interactions which would dominate the spin-orbit coupling in this region should play an equally important role in triggering the fine-structure transitions for this system. The curve crossing region is well separated from the radial coupling region and although there is interesting structure centered at $R_r$ in the adiabatic analysis of Fig. 3 the total cross section is not sensitive to features in the region near and beyond the curve crossing point. Lemoine, Robbe, and Pouilly [14] have argued that large nonadiabatic coupling for $J=100.5$ seen at $R=20.5$ a.u. in Fig. 3(d) indicates a prominent role for the outer radial coupling region. The total cross section is completely insensitive to any features in the outer coupling region and their contention is not supported by our results.

The points $R_r$ and $R_c$ are much closer for Na-Ar than Na-He and the nonadiabatic coupling elements for Na-Ar shown in Fig. 5 peak at the crossing point as anticipated earlier. Just as in the case of the Na+He system (Fig. 3) the coupling matrix elements $G_{12}$ (parity $e$), $G_{13}$ (parity $e$), and $G_{12}$ (parity $f$) have additional structure in the curve crossing region. A magnified plot of the curve crossing region is displayed in the inset. The critical role of the crossing is obvious from Figs. 5(a)–5(c) and the sharp peaks from adiabatic analysis of Fig. 5 isolate a narrow region of potential significance centered at $R_r/R_c$. The sensitivity profiles $\delta \ln\sigma_{1/2\to 3/2}(E)/\delta \ln W_0(R)$ and and $\delta \ln\sigma_{1/2\to 3/2}(E)/\delta \ln W_1(R)$ of Fig. 6 however identify a much broader region of potential significance, and this shortcoming of results from adiabatic analysis is made apparent by Fig. 6(a) where the two-parity resolved sensitivities do indeed have large magnitude at $R_r$, but the total sensitivity being their sum cancels out to essentially zero. This emphasizes the need for care in eliciting insights based on individual parity-resolved results from kinematic analysis of structure in the nonadiabatic coupling matrix elements. The higher frequency and larger domain of ringing structure in Fig. 6(b)–6(d) as compared to that in Fig. 4 for Na-He is due to the larger reduced mass of Na-Ar and greater breadth of the Na-Ar $^2\Pi$ and $^2\Sigma$ wells. As opposed to Na-He, the rotationally induced outer radial coupling is clearly significant for Na-Ar as the maxima in all the sensitivity

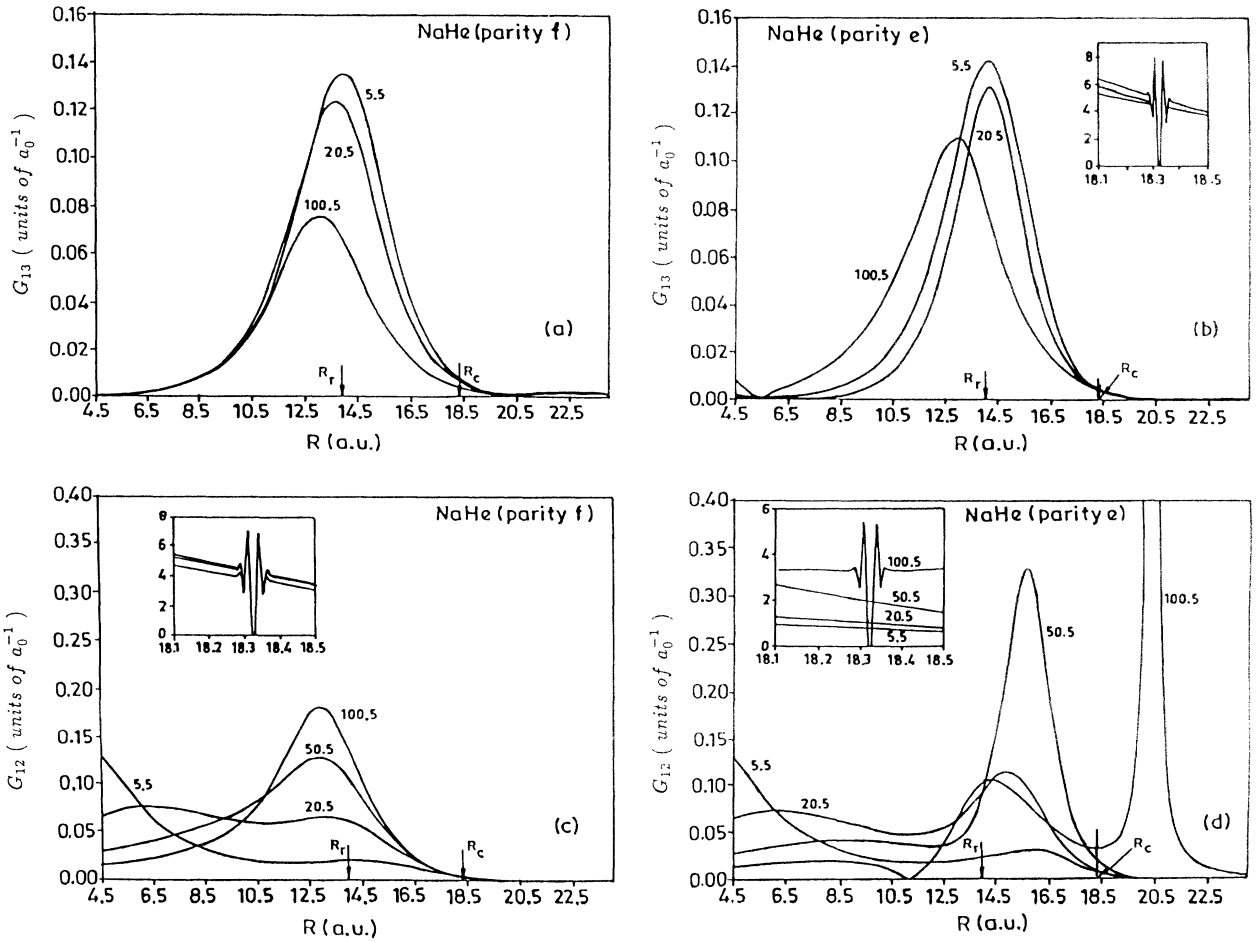


FIG. 3. Dependence on internuclear distance of the absolute values of nonadiabatic matrix elements $G_{13}$ and $G_{12}$ for the collision system Na+He for different values of $J$. A magnified plot of the curve crossing ($R_e=18.33$ a.u.) region is displayed in the inset. The vertical scales in the inset for (b) and (c) are in the units of $10^{-3}$ a.u. and in units of $10^{-2}$ a.u. for (d).

profiles is for $R \simeq 14.60$ a.u. (as compared to $R_r = 11.64$ a.u.) and the sensitivity densities remain nonzero for $R \gg R$. While the nonadiabatic coupling matrix elements from static adiabatic analysis portrayed in Fig. 5 are comparatively parity independent, the contribution from $e$ levels again dominates the dynamic sensitivity profiles. This indicates that a subtle admixture of parity-dependent rotationally induced outer radial coupling and parity independent spin-orbit coupling is responsible for the collisional fine-structure transition $^2P_{1/2} \rightarrow {}^2P_{3/2}$ induced in Na by Ar. The exaggerated role of the curve crossing region as well as the parity independence of the regions of potential significance identified by the adiabatic analysis of Fig. 5 is not seen in the dynamic sensitivity profiles plotted here.

Due to the marked difference between the predictions from the sensitivity and adiabatic analyses, the $\delta\sigma$, $\delta\sigma^e$, and $\delta\sigma^f$ were recalculated by adding an infinitesimal smooth perturbation $\delta V(R)$ to the $^2\Sigma$ curve for the Na-Ar collision and calculating $\sigma(V+\delta V)$ by solving the coupled equations with the modified potential. The $\delta\sigma$ for each $\delta V$ was extracted from $\delta\sigma = \sigma(V+\delta V) - \sigma(V)$. To ensure that the sensitivity densities accurately represent the system dynamics, $\delta\sigma^e$, $\delta\sigma^f$, and $\delta\sigma$ were also calculated using the sensitivity densities reported in Fig. 6 (but without log-normalization) and the same $\delta V(R)$ used in the close-coupling calculations of $\delta\sigma^e$, $\sigma^f$, and $\delta\sigma$. Both the methods produced identical results and those from integration of sensitivity densities are collected in Table I. These results have the same rational trend

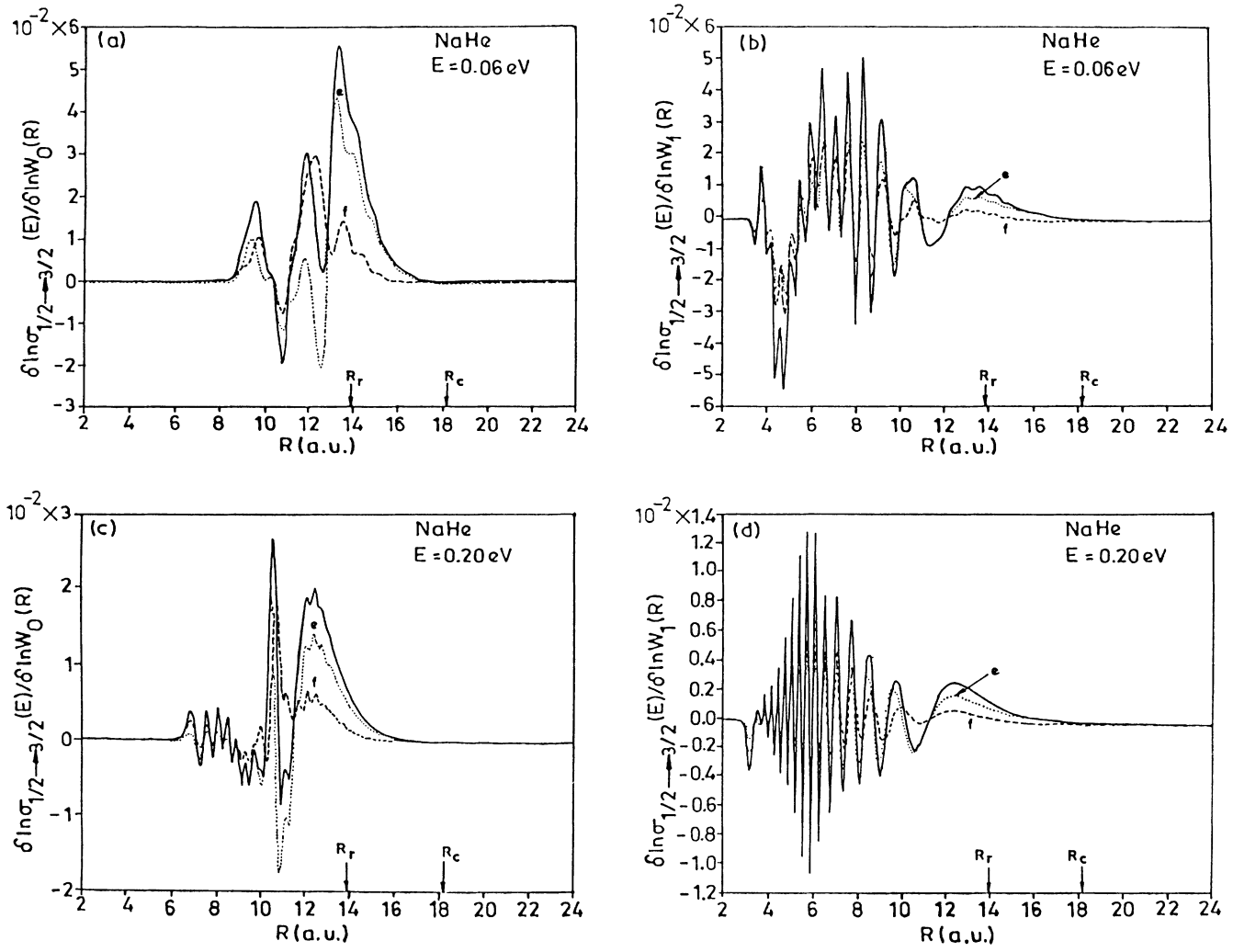


FIG. 4. Sensitivity profiles $\delta \ln\sigma_{1/2\rightarrow 3/2}(E)/\delta \ln W_0(R)$ and $\delta \ln\sigma_{1/2\rightarrow 3/2}(E)/\delta \ln W_1(R)$ at collisional energies $E = 0.06$ and 0.20 a.u. for Na+He. The dynamical dependence of the sensitivities is clearly seen. The area centered around the radial coupling region $R_r$ (10–15 a.u.) seems most important as identified by the adiabatic analysis in Fig. 3 and the contribution from parity $e$ dominates just as in the case of total cross section. The extreme significance of the region centered at $R \simeq 20.5$ a.u. in Fig. 3(d) identified by the static adiabatic analysis is, however, not supported by the dynamic sensitivities plotted here.

between the different regions as those in Fig. 6 except for the sign. The sensitivity densities of Fig. 6 have been multiplied by the potential which is negative over the region of interest and hence produces the sign difference.

The results of Table I independently affirm the conclusions from the sensitivity analysis, e.g., the much greater importance of the regions centered around $R=14.60$ ($R_{\max}$) compared to that for the $R_r$ or $R_c$ regions. Although the individual parity-resolved cross sections from perturbing the potential at $R_c$ are of the same order of magnitude as those from perturbing it at $R_{\max}$ the two add up to produce a sum which is almost two orders of magnitude smaller. The results of the table also reaffirm that the adiabatic analysis has limited utility for identifying the important potential regions.

TABLE I. Values of $\delta\sigma$ for Na-Ar calculated using Eq. (1) by integrating the sensitivity densities reported in Fig. 6 (but without log-normalization) with $\delta V(R)=\eta(1/\sqrt{2\pi\sigma})\exp -[(R-R_0)^2/2\sigma]$. ($\eta=1.0\times10^{-11}$, $\sigma=0.025$, and all values are in atomic units.)

| $R_0$ | 11.64($R_r$) | 12.20($R_e$) | 14.60($R_{\max}$) |
|---|---|---|---|
| $\delta\sigma^e$ | $5.21\times10^{-6}$ | $-1.45\times10^{-5}$ | $-3.60\times10^{-5}$ |
| $\delta\sigma^f$ | $3.34\times10^{-7}$ | $1.36\times10^{-5}$ | $-1.28\times10^{-5}$ |
| $\delta\sigma$ | $5.55\times10^{-6}$ | $-9.14\times10^{-7}$ | $-4.88\times10^{-5}$ |

## IV. CONCLUDING REMARKS

The adiabatic analysis has a long history of offering valuable insights into the mechanism for fine-structure transitions and the specific regions of the underlying curves responsible for this [14]. As argued previously [15], this is, however, based on an energy-independent kinematic analysis of the apparent coupling structure alone. Hidden couplings and subtle interference structure from parity and angular-momentum contributions can be extremely significant and may nullify the results of adiabatic analysis. Some of this is indeed borne out by

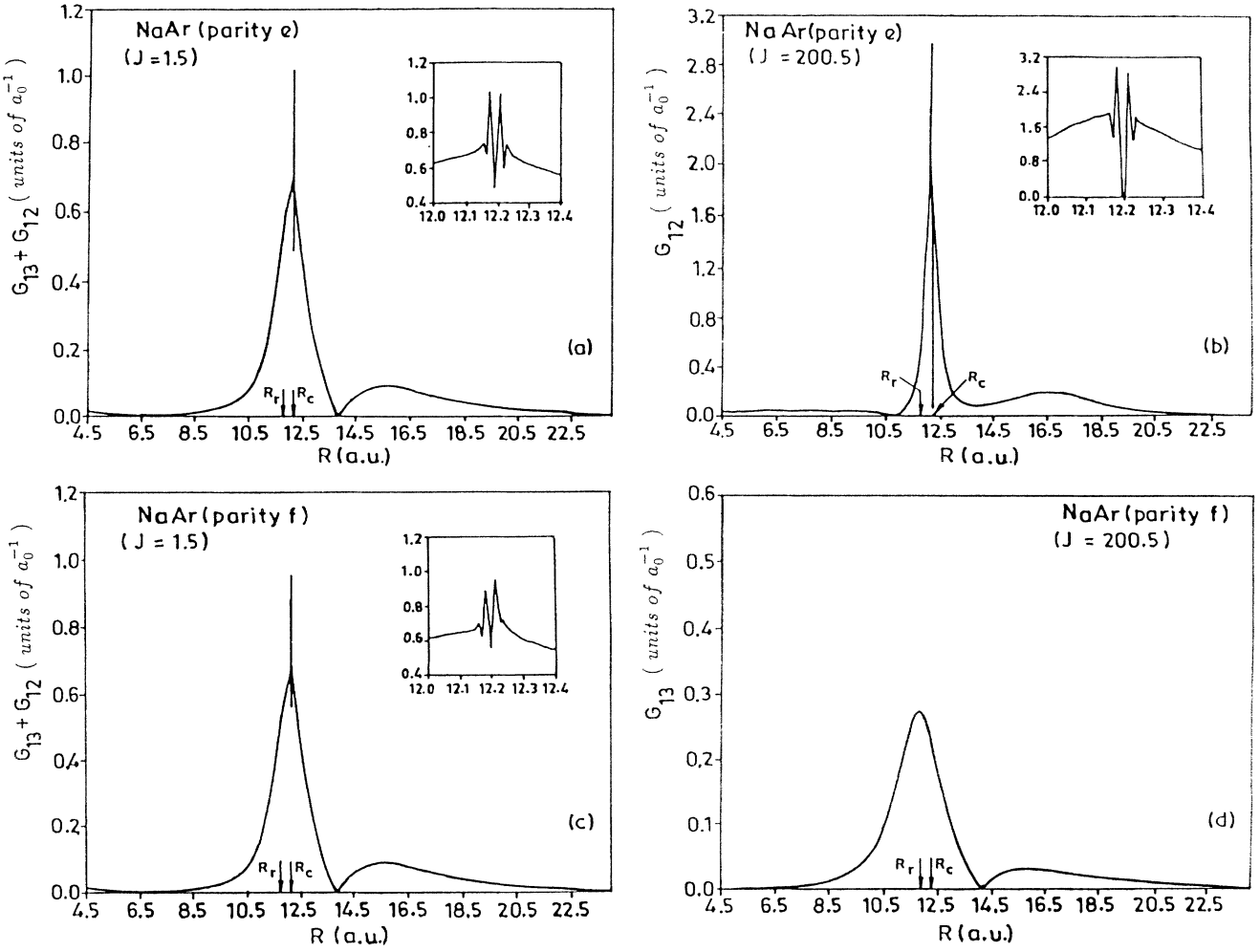


FIG. 5. Dependence on internuclear distance of the absolute values for nonadiabatic matrix elements ($G_{12}+G_{13}$) for $J=1.5$ and $G_{12}$ and $G_{13}$ for $J=200.5$ for the collision system Na+Ar. Just as in the case of the Na+He system (Fig. 3) the coupling matrix elements $G_{12}$ (parity $e$), $G_{13}$ (parity $e$), and $G_{12}$ (parity $f$) have additional structure in the curve crossing region. A magnified plot of the curve crossing region $R_c=12.2$ a.u. is displayed in the inset.

the present analysis where the mechanistic picture brought forth by the energy-independent parity-resolved adiabatic analysis. Some of this is indeed borne out by the present analysis where the mechanistic picture brought forth by the energy-independent parity-resolved adiabatic analysis is seen to be undone by the fully dynamic sensitivity analysis. Furthermore, the adiabatic analysis (1) cannot deconvolute the dependence of collisional cross section on individual potential curves and (2) precludes any energy dependence of the region of potential significance. The sensitivity analysis presented here demonstrates the dynamic dependence of the regions of potential significance and that these differ for the $^2\Sigma$ and $^2\Pi$ curves for both the systems including as a function of energy. The sensitivity densities presented here may also be used as the kernel of an inversion algorithm [30], and an insight into invertibility of the cross-section data is an automatic adjunct of sensitivity analysis. The pronounced ringing structure in the sensitivity profiles for the $^2\Pi$ curve for both the systems and the comparatively small sensitivities at larger $R$ values indicates that the fine-structure transition cross-section data may be less valuable for extracting the $^2\Pi$ potential curves over the well region.

Both adiabatic and sensitivity analyses involve only a minor expense beyond that involved in the routine close-coupling calculation of cross sections themselves and we conclude by emphasizing the complementary role of these two techniques in providing a detailed picture of fine-structure transitions. An adiabatic analysis can be a

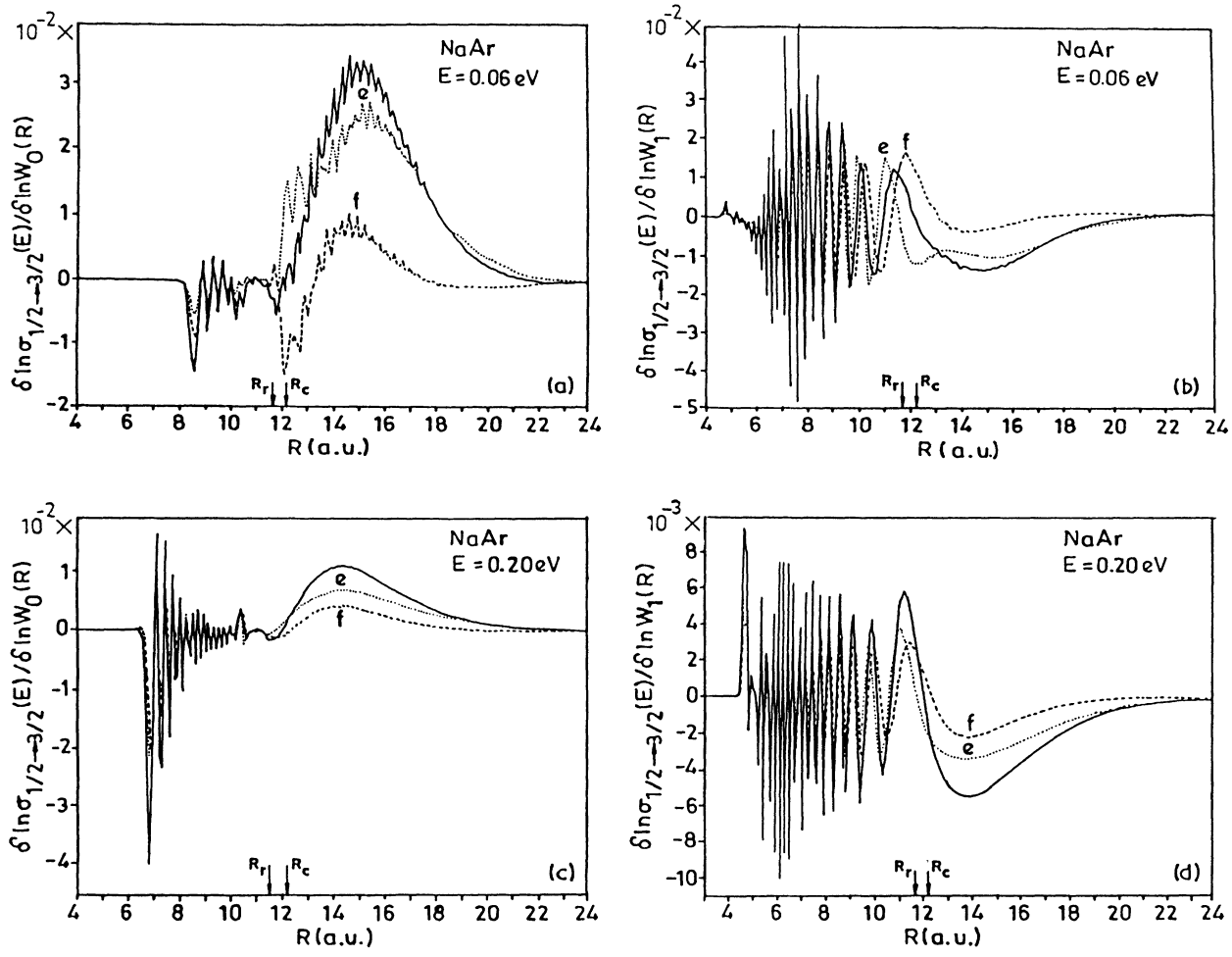


FIG. 6. Sensitivity profiles $\delta \ln\sigma_{1/2\to 3/2}(E)/\delta \ln W_0(R)$ and $\delta \ln\sigma_{1/2\to 3/2}(E)/\delta \ln W_1(R)$ at collisional energies $E=0.06$ and 0.20 a.u. for Na+Ar. The region of potential significance is much broader than that identified by the adiabatic analysis and the area centered around $R_r$ (radial coupling region) does not seem as important as made out by the adiabatic analysis. The sensitivity of the cross section in the region 14 to 18 a.u. indicates that the outer radial coupling region is most important. The exaggerated role of the curve crossing region as well as the parity independence of the regions of potential significance identified by the adiabatic analysis of Fig. 5 are not seen in the dynamic sensitivity profiles plotted here.

useful first step, but a complete picture of what regions are important can only be revealed by a dynamical sensitivity analysis.

## ACKNOWLEDGMENTS

We are grateful to Dr. B. Pouilly for making available the $^2\Sigma$ and $^2\Pi$ curves for Na-He and Na-Ar used in our calculations. This investigation has been sponsored by the Board for Research in Nuclear Sciences of the Department of Atomic Energy, India, through their Grant No. 37/16/89-G to M.K.M. Their support is gratefully acknowledged. The author H.R. acknowledges support from the U.S. Department of Energy. D.A.P. is grateful to the CSIR, India, for financial support [Grant No. 9/87(161)/93 EMR-I].

[1] R. H. G. Reid, J. Phys. B **6**, 2018 (1973).
[2] J. M. Launnay and E. Roueff, J. Phys. B **10**, 879 (1977).
[3] D. E. Fitz and D. J. Kouri, J. Chem. Phys. **73**, 5115 (1980).
[4] M. H. Alexander and B. Pouilly, in *Selectivity in Chemical Reactions,* edited by J. C. Whitehead (Kluwer Academic, Dordrecht, 1988), and references therein.
[5] M. H. Alexander, in *Gas Phase Chemiluminescence and Chemi-Ionization,* edited by A. Fontijn (Elsevier, New York, 1985).
[6] M. H. Alexander, J. Chem. Phys. **96**, 6672 (1992).
[7] T. Orlikowski and M. H. Alexander, J. Phys. B **17**, 2269 (1984); B. Pouilly, T. Orlikowski, and M. H. Alexander, J. Phys. B **18**, 1953 (1985).
[8] B. Pouilly and M. H. Alexander, J. Chem. Phys. **86**, 4790 (1987).
[9] E. E. Nikitin, J. Chem. Phys. **43**, 744 (1965); Adv. Chem. Phys. **28**, 317 (1975); E. E. Nikitin and S. Ya Umanskii, *Theory of Slow Atomic Collisions* (Springer, Berlin, 1984).
[10] E. I. Dashevskaya, E. E. Nikitin, and A. I. Reznikov, J. Chem. Phys. **53**, 1175 (1970).
[11] R. K. Preston, C. Sloane, and W. H. Miller, J. Chem. Phys. **60**, 4961 (1974).
[12] R. W. Anderson, J. Chem. Phys. **77**, 5246 (1982).
[13] M. H. Alexander, T. Orlikowski, and J. E. Straub, Phys. Rev. A **28**, 73 (1983), and references therein.
[14] D. Lemoine, J. M. Robbe, and B. Pouilly, J. Phys. B **21**, 1007 (1988).
[15] D. A. Padmavathi, M. K. Mishra, and H. Rabitz, Chem. Phys. **179**, 469 (1994).
[16] V. Aquilanti and G. Grossi, J. Chem. Phys. **73**, 1165 (1980).
[17] V. Aquilanti, P. Cassavecchia, G. Grossi, and A. Lagana, J. Chem. Phys. **73**, 1173 (1980).
[18] F. Masnou-Seeuws and R. MacCarrol, J. Phys. B 7, 2230 (1974).
[19] S. Shi and H. Rabitz, Comp. Phys. Rep. **10**, 1 (1989).
[20] D. A. Padmavathi, M. K. Mishra, and H. Rabitz, Phys. Rev. A **48**, 279 (1993).
[21] D. A. Padmavathi, M. K. Mishra, and H. Rabitz, Phys. Rev. A **48**, 286 (1993).
[22] M. J. Smith, S. Shi, and H. Rabitz, J. Chem. Phys. **91**, 1051 (1989).
[23] M. Mishra, R. Guzman, and H. Rabitz, Phys. Rev. A **36**, 1124 (1987).
[24] R. P. Saxon, R. E. Olson, and B. Liu, J. Chem. Phys. **67**, 4961 (1974).
[25] J. Pascale and R. E. Olson, J. Chem. Phys. **64**, 3538 (1976).
[26] A. D. Wilson and Y. Shimoni, J. Phys. B **7**, 1543 (1974).
[27] F. H. Mies, Phys. Rev. A **7**, 942 (1973); **7**, 957 (1973).
[28] J. M. Brown, J. T. Hougen, K. P. Huber, J. W. C. Johns, I. Kopp, H. Lefebvre-Brion, A. J. Meref, D. A. Ramsay, J. Rostas, and R. N. Zare, J. Mol. Spectrosc. **55**, 500 (1975).
[29] See Table I of Ref. [14].
[30] T. S. Ho and H. Rabitz, J. Chem. Phys. **89**, 5614 (1988); **91**, 7590 (1989); **94**, 2305 (1991); **96**, 7092 (1992); H. Heo, T. S. Ho, K. Lehmann, and H. Rabitz **97**, 852 (1992); R. Boyd, T. S. Ho, H. Rabitz, D. A. Padmavathi, and M. K. Mishra (unpublished).